Fatigue performance evaluation of a Nickel-free titanium-based alloy for biomedical application - Effect of thermomechanical treatments

Geneviève Mussot-Hoinard, Wafa Elmay, Laurent Peltier, Pascal Laheurte

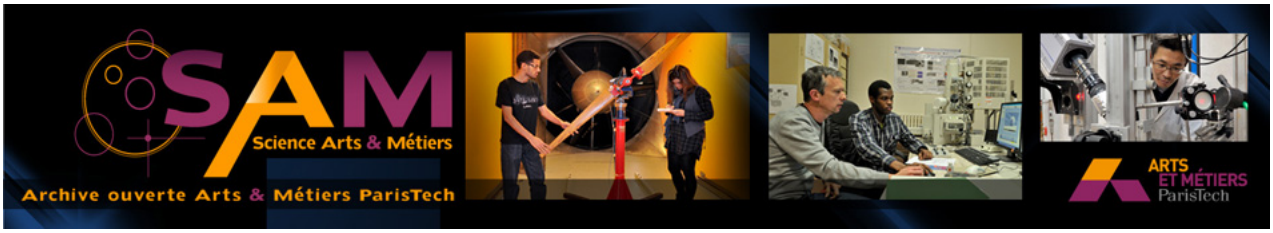

Fatigue performance evaluation of a Nickel-free titanium-based alloy for biomedical application - Effect of thermomechanical treatments

G. Mussot-Hoinard[a,*], W. Elmay[a], L. Peltier[b], P. Laheurte[a]

[a] *Laboratoire d'Etude des Microstructures et de Mécanique des Matériaux (LEM3 UMR CNRS 7239), Université de Lorraine, île du Saulcy, 57045 Metz Cedex, France*

[b] *ENSAM, 4 Rue Augustin Fresnel, 57070 Metz, France*

A B S T R A C T

In the present work, structural fatigue experiments were performed on a Ti-26Nb alloy subjected to different thermomechanical treatments: a severe cold rolling, a solution treatment and two aging treatments at low-temperature conducted after cold rolling in order to optimize the kinetics of precipitation. The aim is to investigate the effect of microstructural refinement obtained by these processes on fatigue performances.

Preliminary tensile tests were performed on each state and analyzed in terms of the microstructure documented by using X-Ray diffraction and TEM analysis. These tests clearly promote the short-time-aged cold-rolled state with a fine α and ω phases precipitation. An interesting balance between mechanical properties such as high strength and low Young's modulus has been obtained.

Cyclic bending tests were carried out in air at 0.5%, 1%, 2% and 3% imposed strain amplitudes. At low straining amplitude, where the fatigue performances are at their best, the cold-rolled state does not break at 3×10^6 cycles and the long-time aged precipitation hardened state seems to be a good competitor compared to the cold-rolled state.

All failure characteristics are documented by Scanning Electron Microscopy (SEM) micrographs and analyzed in term of microstructure.

1. Introduction

Due to their attractive mechanical properties, corrosion resistance and excellent cold workability, biocompatible (Williams, 2008) metastable β-titanium alloys have attracted much attention for medical applications. During the last decade, Nickel-free low modulus β-titanium alloys were developed and characterized. Efforts were made through many studies to improve their properties in order to fulfill the application requirements (Hanada et al., 2005; Kim et al., 2006; Miyazaki et al., 2006; Geetha et al., 2009; Guo et al., 2010; Li et al., 2011; Niinomi et al., 2012). In particular, the refinement of the microstructure through thermomechanical treatments was given as an efficient way to improve the mechanical properties (Kim et al., 2006; Elmay et al., 2013; Elmay et al., 2014). Thus, low-temperature associated to short-time aging treatment performed on severe cold deformed material contributes to an interesting combination of high strength, large recoverable strain and low elastic modulus.

Furthermore, most devices used for biomedical applications are solicited under fatigue conditions. Therefore, the characterization of the fatigue behavior is nowadays a major investigation for biomaterials titanium alloys in order to evaluate their durability and their reliability. Many authors have contributed to a better understanding of fatigue behavior of titanium alloys. Some under rotating-bending mode (Miyazaki et al., 1999; Wagner et al., 2004; Young and Van Vliet, 2005; Bahia et al., 2006; Figueiredo et al., 2009; Pelton et al. 2013), others under three-point bending mode (Xue et al., 2007; Bourauel et al., 2008). Some authors have also worked on the fatigue performance of non-toxic Nickel-free Titanium alloys by performing cycling under tension mode (Akahori et al., 2005; Boehlert et al., 2005; Niinomi, 2003; Niinomi et al., 2007; Niinomi, 2007; Boehlert et al., 2008; Frotscher et al., 2009; Tahara et al., 2009; Zhang et al., 2009; Song et al., 2015; Sheremetyev et al., 2016). An evaluation of fatigue performance of aged materials beforehand solution treated has been the subject of the majority of these different studies. Few of these authors have considered the effect of aging treatments after cold-rolling (Akahori et al., 2005; Niinomi, 2007). However, the effect of aging time and more particularly of a short-treatment has not been taken into account. For instance, in these studies, long times aging are investigated (28.8 ks for Boehlert et al., 2005 and 259.2 ks for Akahori et al., 2005). The operating conditions and materials being different, a result

comparison is not conceivable.

In the present study, the bending mode was chosen to characterize the fatigue life of a Ni-free biocompatible β-titanium alloy. This mode is appropriate for the fatigue of bone-plates and fixation devices commonly used for complicated fractures (Niinomi and Nakai, 2011). The selected Ni-free biocompatible β-titanium alloy was the Ti-26Nb alloy (at%). Bending straining was carried out on four metallurgical states: a severe hardening by cold rolling (CR), a solution treatment (ST) followed by water quenching (WQ) and two aging treatments conducted after severe hardening, at a low temperature of 573 K for two different aging times, a short one at 0.6 ks and a twelve time longer one at 7.2 ks. The low aging temperature associated to the short-time treatment has a nanostructuring effect of the ω and/or α phases precipitation occurring during aging of β-titanium alloys. These precipitates have an influence on the stability of the β phase; Limiting their coarsening leads to the obtaining of nanoscaled phases with a fine dispersion and a low volume fraction allowing the limitation of detrimental effects such as a loss of ductility and an increase in elastic modulus (Ohmori et al., 1998; Sun et al. 2011; Elmay et al., 2014).

Finally, this paper has to be considered as a contribution to a better understanding of the effect of microstructural refinement and nanoscaled precipitates obtained by thermomechanical processing on the fatigue life and the fracture characteristics of Ni-free β- titanium alloys.

2. Experimental procedure

2.1. Material

A Ti-26Nb (at%) ingot was obtained using the cold crucible levitation melting technique (CCLM) under high purity Ar atmosphere using ultra-pure titanium and niobium raw materials (Morita et al., 2000). This ingot was then subjected to a thermal homogenization treatment at 1223 K during 72 ks under high purity Ar atmosphere followed by water quenching. A severe cold rolling (CR) process was performed on the Ti-26Nb homogenized ingot. The achieved cold rolling thickness reduction rate was about 95% nominal strain. The material was flat bars with a rectangular cross section of width and height (b and h) respectively equal to 1.88 mm and 0.8 mm ± 0.04 mm. The longitudinal direction of the bars was parallel to the rolling direction.

Four states were investigated for the present study: a cold rolled state issued from the severe cold rolling process previously described, a solution treated state and two cold rolled aging states. The solution treated state was obtained by a solution treatment (ST) performed above the β transus at 1173 K for 3.6 ks on the cold rolled sample and then water quenched. Concerning aging treatments, most authors make the choice to apply them after a ST state (Akahori et al., 2005; Boehlert et al., 2005; Niinomi, 2007; Niinomi et al., 2007; Boehlert et al., 2008; Frotscher et al., 2009; Tahara et al., 2009; Zhang et al., 2009; Song et al., 2015). In the present study, the aging treatments were applied after the CR process in order to get maximum benefit from the hyperdeformed structure in which nucleation sites promote the kinetic precipitation of new phases (Furuhara et al., 2001) leading to improve hardening. Aging treatments were conducted under ultra pure Ar atmosphere at a low temperature of 573 K for either a short time period of 0.6 ks or a twelve time longer period of 7.2 ks. These treatments were followed by water quenching (WQ). These four states were respectively called CR, CR/ST/WQ, CR/573K-0.6ks/WQ and CR/573K-7.2ks/WQ.

Surface roughness of samples was measured by a Leica confocal and interferometry 3D microscope. For each of the four states, the mean transverse value, determined from three different regions on samples, is less than 0.5 μm. The samples surface was therefore left without polishing. An X-Ray diffractometer equipped with curved position sensitive detector with Cu-Ka radiation was used to identify the different phases present in the samples after the different thermo-mechanical treatments. Thin foils were extracted from flat bars using a FIB Zeiss Auriga 40 equipped with both electronic and ionic columns (Gemini and Orsay Physics Cobra, repectively). An ionic Ga beam of 30 kV was used. Thin foils were finished under a beam of 5 kV before extraction in order to eliminate amorphous layers induced by the high energy abrasion. Microstructure observations were done using a Philips transmission electron microscopy (TEM) operating at 200 kV.

The failure characteristics were analyzed using a Scanning Electron Microscopy (SEM) operating at an acceleration voltage of 30 kV.

2.2. Experimental testing

Bending fatigue tests complemented by preliminary common tensile tests were undertaken on the four CR, CR/ST/WQ, CR/573K-0.6ks/WQ and CR/573K-7.2ks/WQ states in order to identify the best candidate to medical applications.

2.2.1. Preliminary tensile testing

Room temperature uniaxial tensile tests up to 3% strain were performed at a strain rate of 2×10^{-3} s^{-1} using a Zwick testing machine. Tensile direction was parallel to the rolling direction and strain was measured with an extensometer.

2.2.2. Bending fatigue testing

Bending testing is appropriate for the study of the fatigue life of bone-plates and fixation devices commonly used for complicated fractures.

Fatigue tests were conducted at room temperature using a bending set-up and an automated servo-hydraulic MTS mechanical testing machine equipped with a 0.25 kN force transducer adapted to the specimens answer. The cyclic mechanical strain were applied to the specimen by cyclical compressive displacements using a sinusoidal profile at a frequency of 5 Hz. Fatigue tests were undertaken at 3%, 2%, 1% and 0.5% maximum strain amplitudes on sample surfaces by using respectively, according to relation (1), loading cylinders of 13.3 mm, 20 mm, 40 mm, and 80 mm radii of curvature R. The values of the compressive displacements necessary to obtain the required strain amplitude have been experimentally verified for each cylinder using a strain gauge placed on the specimen surface.

$$\varepsilon = h/2R \tag{1}$$

(Eggeler et al.,2004; Wagner et al.,2004; Pelton et al., 2013)

The maximum stress $\sigma_{xx\max}$ (relation 2) due to the bending moment M in the central section of the sample never exceed 250 MPa. I_z represents the second moment of area with respect to the vertical axis.

$$|\sigma_{xx}|_{\max} = h\ M/2\ I_z \tag{2}$$

The fatigue limit, at which the specimen did not break, was set at 3×10^6 cycles in this study. A standard hip-joint should be able to support about 2×10^6 cycles per year (Windler and Klabunde, 2001). For each state, all fatigue tests were performed twice or more in case of scattering of the results.

Some fatigue tests were instrumented with a FLIR infrared thermal camera in order to verify the adiabatic condition during the fatigue tests. No representative variation in temperature (below 1 K) has been registered.

All tests were instrumented with a Microsoft HD camera taking views at 1 min shooting interval to detect precisely the failure moment of samples. Therefore, this approach allowing real-time monitoring of the test can be considered as an in-situ method compared to other methods commonly used such as low current detection.

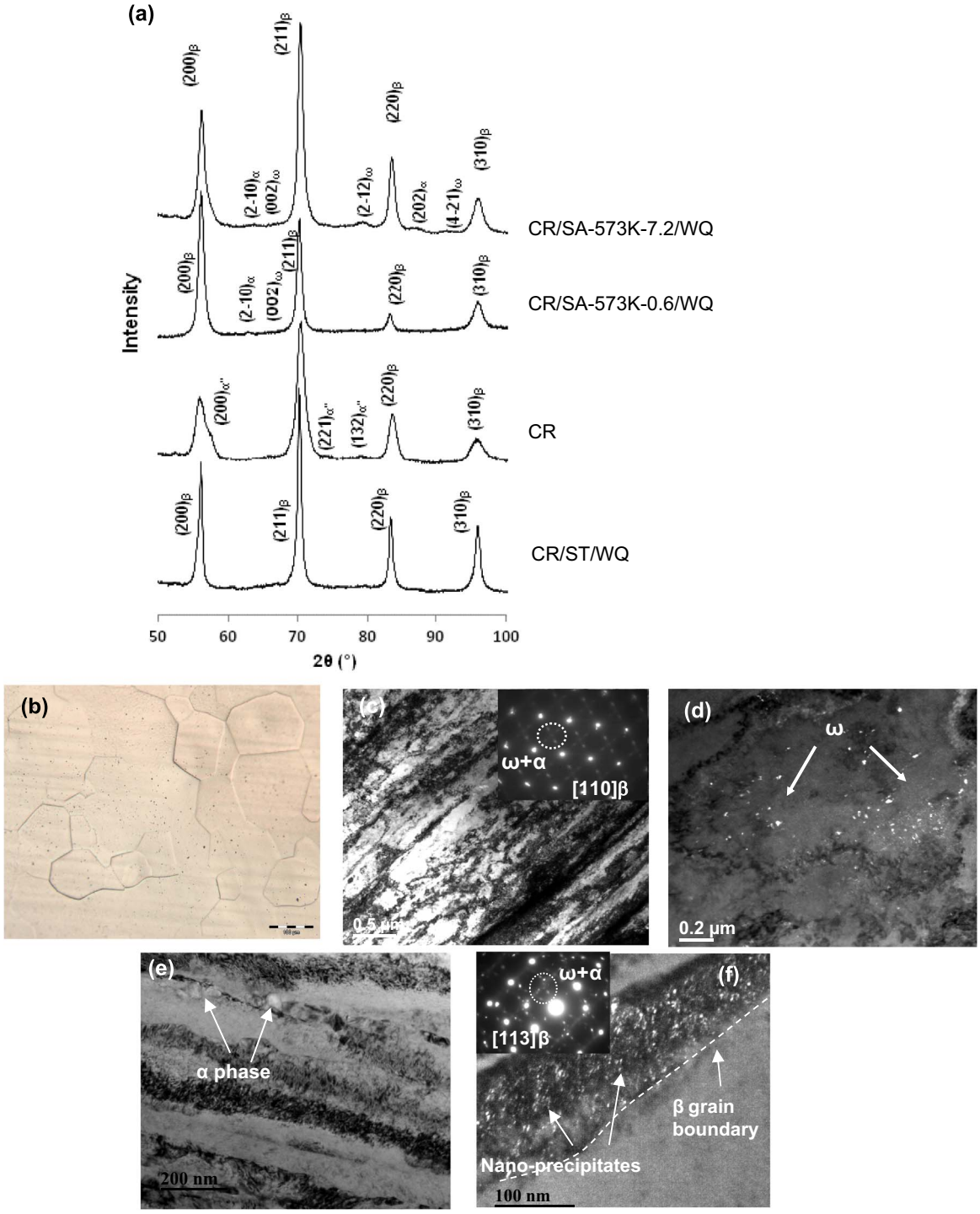

Fig. 1. (a) X-Ray diffraction profiles obtained for the CR, CR/ST/WQ, CR/573K-0.6ks/WQ, and CR/573K-7.2ks/WQ Ti-26Nb specimens, (b) microstructure obtained for the CR/ST/WQ specimen, (c) and (d) TEM micrographs of the CR/573K-0.6ks/WQ specimen with bright field image of obtained microstructure and the corresponding diffraction pattern along $[110]_\beta$ zone axis and dark field image showing nano-sized ω precipitates and (e) and (f) TEM micrographs of the CR/573K-7.2ks/WQ specimen with bright field image of obtained microstructure and the corresponding diffraction pattern along $[113]_\beta$ zone axis and dark field image showing nano-precipitates.

3. Results and discussion

3.1. Microstructure

XRD analyses (Fig. 1a) were carried out on the four states in order to identify the present phases engendered by the different thermo-mechanical treatments. To characterize the microstructure more precisely, XRD results were complemented by optical micrograph and TEM images for the solution treated (Fig. 1b), the CR/573K-0.6ks/WQ aged specimen (Fig. 1c and Fig. 1d) and the CR/573K-7.2ks/WQ aged specimen (Fig. 1e and Fig. 1f).

According to the XRD pattern, the initial CR state revealed the presence of both β phase and α" stress-induced martensite (Fig. 1a). For the solution treated specimen (ST), the α" phase completely disappeared and only the β phase is detected (Fig. 1a). The athermal ω phase usually obtained during quenching is not observed. It is reported that athermal ω phase precipitation depends on annealing temperature before quenching (Prima et al., 2000a, 2000b). The

Table 1
Table summarizing the microstructure engendered by the different thermomechanical treatments.

Ti-26Nb states	Microstructure
CR	Hyperdeformed β phase+ Stress-induced martensite α" + many crystal defects
CR/573 K (0.6 ks/WQ and 7.2 ks/WQ)	Hyperdeformed β phase + (α + ω) nanoprecipitates
CR/ST/WQ	Recrystallized β phase - grains of 80–100 μm

recrystallized β-grains size is of about 80–100 μm according to the optical micrograph (Fig. 1b). For the Ti-26Nb alloy aged at 573 K after cold rolling, the α" phase has completely disappeared and a coexistence of β, ω and α phases is observed on the XRD patterns of both aging times samples (Fig. 1a). TEM micrographs on the aged alloy at 573 K (Fig. 1c and Fig. 1e) revealed a deformed microstructure with elongated blocks identified as β domains, as well as many crystal defects which could be considered as nucleation sites for the secondary phases.TEM micrographs confirmed the precipitation of the ω and α phases.

These results are in agreement with literature results for the Ti-23Nb-0.7Ta-2Zr (TNTZ) titanium alloy (Akahori et al., 2005). It has also been reported that a cold rolled β/α" metastable β-titanium alloy can be subjected, via easily homogeneous lattice deformation, to the successive α"→β→ω transformations, during aging in the range of 473–673 K (Ohmori et al., 1998). The observed ω phase has to be only related to the isothermal ω phase (Silcock, 1958**;** Froes et al., 1980). This phase has been represented by a core depleted in Nb and surrounded by a β area slightly more rich in Nb than the β matrix in Ti-Nb alloys (Lyon, 1981). Indeed, during the course of aging, the isothermal ω precipitates formation is controlled by the enrichment of the β matrix with the alloying element (Hickman, 1969). Thus, it increases the β phase stability (Duerig and Williams, 1980; Hao et al., 2007**;** Kent et al., 2010**;** Elmay et al., 2013) and therefore the transforming driving force needed to induce the α" martensitic phase is increased (Moffat and Larbalestier, 1988; Ohmori et al., 1998; Ohmori et al., 2001).

The α phase formation during aging for β-titanium alloys has also well been observed by different authors. However, its training mode presents a lack of agreement in the literature. It has been suggested that the ω phase acts as the precursor of the α phase either through a direct way, transforming itself into α phase (Hickman, 1969; Froes et al., 1980) or in an indirect way involving either a single mechanism (Ohmori et al., 1998; Ohmori et al., 2001) or a twin mechanism (Prima et al., 2000a, 2000b). According to the single mechanism, the α phase would nucleate at the ω/β interfaces by consuming the ω phase during the course of aging (Ohmori et al. 1998; Ohmori et al., 2001). According to the double mechanism, the α phase would involve both a displacive ω→β reversion at intermediate aging temperature and the precipitation of α phase in the depleted areas β-stabilizer of the β-matrix (Prima et al. 2000b). One can however note that for a Ti-26Nb alloy aged at 573 K being firstly solution treated, the β+ω microstructure has only been observed (Moffat and Larbalestier, 1988).

It has also been reported that direct α phase should be promoted due to the heterogeneous nucleation sites (dislocations or subboundaries) resulting from the processing history (Froes et al., 1980). Some studies highlight the formation of direct α phase in form of round precipitates at β grain boundaries ("necklace" microstructure) for β titanium alloys subjected to a thermomechanical processing (Sauer and Luetjering, 2001**;** Xu et al., 2016**)**. Heterogeneous direct α phase has also been observed at β grains boundaries for a solution-treated Ti-Mo-Fe-Al alloy aged above 663 K. The spheroidization of the α phase was obtained under continued aging (Azimzadeh and Rack, 1998).

For the short-time aged specimen, the ω and α phases precipitates are in low proportion in view of their weak intensity spots (surrounded by white circle, in the diffraction pattern, Fig. 1c). It is important to note that spots intensity corresponding to these phases (surrounded by white circle in the diffraction pattern, Fig. 1e) is higher for longer isothermal holding of 7.2 ks at 573 K than those observed for short-time aging which confirms a higher volume fraction of these precipitates. This result is in agreement with XRD results (Fig. 1a) showing additional peaks of both phases.

The intragranular ω precipitates observed on Fig. 1d and Fig. 1f have an ellipsoidal morphology and their size along the major axis is of about 10–20 nm for the short-time aging (0.6 ks) and of about 3–5 nm for the longer-time one (7.2 ks). The ω particles size decreases with the increasing of the isothermal holding time while the volume fraction of the α phase increases. This observation suggests that ω phase could gradually be replaced by α phase leading to a smaller precipitation with the increase of the aging time which is in agreement with the precursor role of ω phase in the formation of α phase during isothermal holding (Prima et al., 2006).

Furthermore, it is important to note that the α phase particles of about 40–60 nm is observed along the β grain boundaries for the hyper-deformed microstructure aged at 573 K during 7.2 ks (Fig. 1e).

The microstructures engendered by the different thermomechanical treatments are summarized in Table 1.

3.2. Preliminary tensile testing

The stress-strain tensile curves up to 3% of the CR, CR/573K-0.6ks/WQ, CR/573K-7.2ks/WQ and CR/ST/WQ states, presented in Fig. 2, clearly show the great influence of the thermo-mechanical treatments on the mechanical properties. A focus concerning the evolution of the incipient elastic modulus E (defined by the slope of the tangent at zero stress as shown in Fig. 2**)**, the critical stress for induced martensite $\sigma_{c(im)}$, the critical stress for slip σ_{cs} and the rupture when it is present is given in the light of the microstructural results and more specifically with regard to the stability of the β phase. The mechanical properties are reported in Table 2.

The solution-treated specimen displays a Young's modulus of about 48 GPa which is quite close to that of the cortical bone (max 27 GPa). A first deformation mechanism corresponding to reversible stress-induced martensite is occurring from the metastable β phase (Kim et al., 2007) at the required critical induced martensite stress, $\sigma_{c(im)}$, of about 360 MPa (Fig. 2) followed by martensite variant reorientation (Liu and Xiang, 1998). A second mechanism referring to plasticity appears at 2.5% strain at a critical stress for slip, σ_{cs}, of about 600 MPa.

The cold rolled CR state is characterized by an incipient elastic modulus of 54 GPa slightly superior to that of the solution treated-specimen and an enhanced critical stress for slip deformation, σ_{cs}, of about 900 MPa at around 2% strain. These results have to be linked to the presence of the many crystal defects introduced within the β phase having the effect to block the dislocation motion.

The results obtained for aged specimens at 573 K highlight the strong dependence of the mechanical properties on the aging time and consequently the influence of the volume fraction of the (α + ω) phases. The relative elastic modulus according to the different phases has been established as follow: $E_\beta < E_\alpha < E_\omega$ (Bowen,1971; Larson and Zarkades,1974).

At short-time aging (0.6 ks), the elastic modulus does not vary significantly compared to that of the initial cold rolled state which is consistent with the TEM results showing a low volume fraction of the α + ω precipitates. However, for twelve time longer aging (7.2 ks), the elastic modulus is about 1.5 times higher (68 GPa) which is due to a higher volume fraction of the (α + ω) nanoscale precipitates.

Furthermore, the amount of ω and α phases in the aged alloys caused a substantial improvement of the critical stress for slip, σ_{cs}, with respect to aging time. Compared to the critical stress for slip of the CR

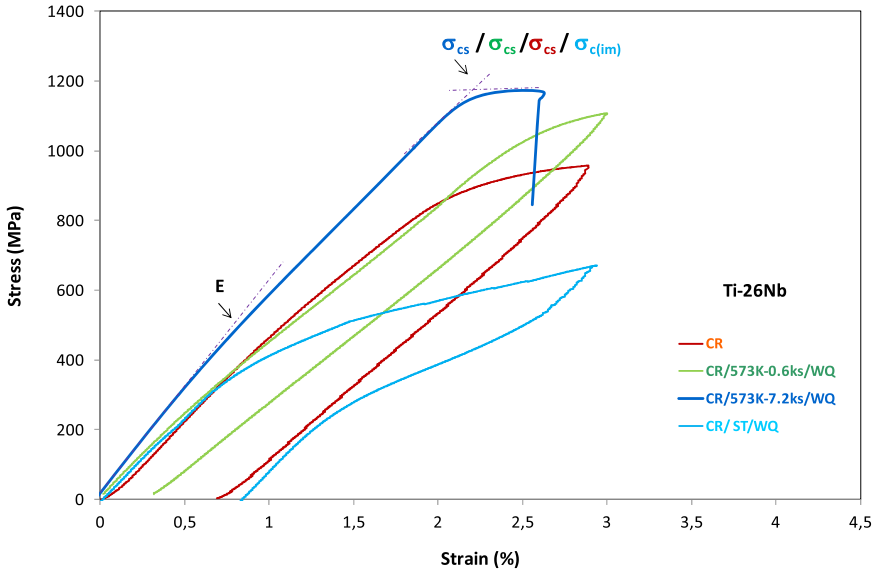

Fig. 2. Stress-strain curves up to 3% strain CR, CR/573K-0.6ks/WQ, CR/573K-7.2ks/WQ and CR/ST/WQ Ti-26Nb specimens under uniaxial tensile tests performed at room temperature.

state (900 MPa), the improvement is of about 16% (1052 MPa) and 32% (1192 MPa) for respectively the 0.6 ks and 7.2 ks aging-time states. According to literature, the α phase increases the yield stress to a lesser extent than the ω phase (Williams et al., 1971).

Finally, a plastic deformation occurred in the case of the low-time aging (0.6 ks) while a sudden break was observed at low macroscopic strain (< 3%) in the case of the longer time aging (7.2 ks). This later state with smaller ω particles and a larger amount of α phase observed at β grains boundary has indeed failed at low strain amplitude and its post-mortem SEM micrograph (Fig. 3) shows a dimpled morphology, which is characteristic of fast ductile fracture.

The preliminary up to 3% strain common tensile tests undertaken on the CR, CR/573K-0.6ks/WQ, CR/573K-7.2ks/WQ and CR/ST/WQ states clearly promote the short-time aged β-titanium alloy. However, this first result has to be confirmed by fatigue life results.

3.3. Bending fatigue testing

3.3.1. Fatigue life results

Fatigue life results, represented by a plot of strain amplitude ε_a versus number of cycles to failure, log N_f (Fig. 4), are quite reproducible and show a thermo-mechanical treatments dependence. The fatigue limit, at which the specimen was declared not failed, was set at 3×10^6 cycles. The regions below and upon 10^5 cycles correspond respectively to the Low and the High Cycle Fatigue (LCF, HCF) life regions.

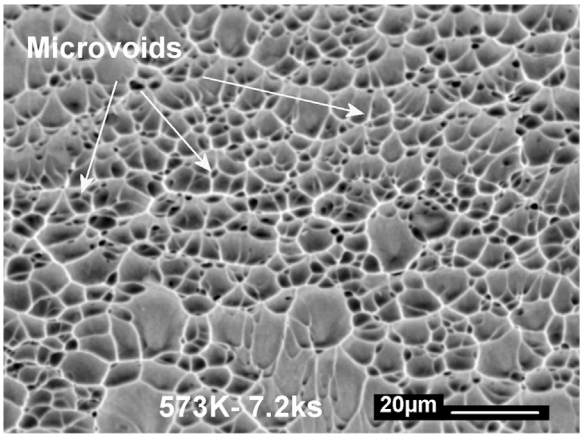

Fig. 3. SEM micrograph of CR/573K-7.2ks/WQ post-mortem specimen showing microvoids characteristic of a rapid ductile fracture.

The solution treated specimen displays the lowest fatigue performances by remaining in the LCF life region even for tests performed at 0.5% maximum strain amplitude.

It is important to bear in mind that for this state the first deformation mechanism is the reversible β↔α" martensitic transformation. Therefore, cycling under this reversible mechanism has the

Table 2
Mechanical properties obtained after 3% strain for CR, CR/573K-0.6ks/WQ, CR/573K-7.2ks/WQ and CR/ST/WQ Ti-26Nb specimens.

Tensile Mechanical Properties	**Ti-26Nb States**		
	CR	**CR/573K-0.6ks/WQ** **CR/573K-7.2ks/WQ**	**CR/ST/WQ**
Incipient elastic modulus E (± 3 GPa)	~ 54	~ 45 (0.6 ks) ~ 68 (7.2 ks)	~ 48
Critical stress for induced martensite $\sigma_{c(im)}$ (± 5 MPa)	–	–	360
Critical stress for slip σ_{cs} (MPa)	904	1052 (0.6 ks) 1190 (7.2 ks)	> 600
Rupture (up to 3% strain)	–	at ~ 2.6% (7.2 ks)	–

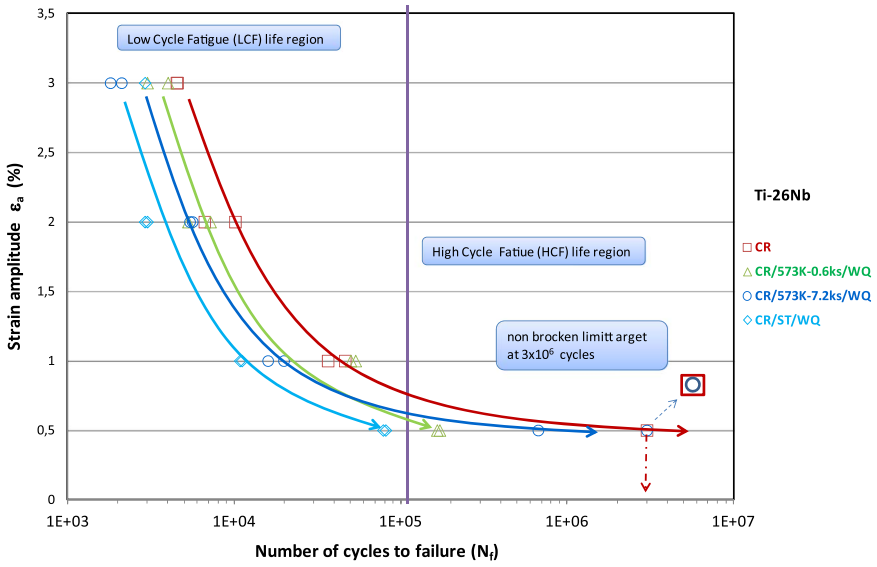

Fig. 4. Fatigue life results of Ti-26Nb flat bars under bending fatigue in air.

effect of localizing deformation, and thus reaching the plastic domain faster. The critical stress for induced martensite under present bending cycling is determined relatively lower (≤ 250 MPa) than that under tensile curves (360 MPa). However, it has been reported that during cycling under tension, the transformation stress of solution treated alloys decreases from the first loading cycles (Kim et al., 2006; Tahara et al., 2009). This latter result applied to a bending cycling justifies the fact that the phase transformation could be reached at the low value of about 250 MPa.

The cold rolled (CR) and cold rolled aged (CR/573K-0.6ks/WQ and CR/573K-7.2ks/WQ) specimen revealing a strong hardening under tension have quite close fatigue life performances under 3%, 2% and 1% strain amplitude, and exhibit high fatigue resistance at 0.5% strain. More than 3×10^6 cycles have been achieved for the CR specimen. For the cold-rolled short-time (0.6 ks) aged specimens, this performance drops to the mean value of 1.7×10^5 cycles. Furthermore, in the case of the twelve time longer (7.2 ks) aged specimens, the performances are well improved with a dispersion, confirmed by supplemented tests, from 6.7×10^5 cycles to more than 3×10^6 cycles.

Fatigue results established that the short-time aged (0.6 ks) cold-rolled specimen that was the best candidate under tension testing (best compromise between elastic modulus, Yield stress and deformation), finally has low fatigue performances compared to that of the CR and CR/573K-7.2ks/WQ sates.

The cold rolled specimen (CR) which exhibits residual stress and many crystal defects, enhanced in a reproducible manner the fatigue performances by a factor greater than 50 compared to that of the CR/573K-0.6ks/WQ state. Considering its mechanical properties, which are quite satisfactory under tension, as well as this excellent fatigue performance, the Ti-26Nb alloy at this state could be a good candidate for biomedical applications.

These results are supplemented by further data on macroscopic fracture and SEM micrographs.

3.3.2. *Macroscopic fatigue fracture*

Table 3 describes the macroscopic fatigue fracture for each of the

Table 3
Description of macroscopic failure for the CR, CR/573K-0.6ks/WQ, CR/573K-7.2ks/WQ and CR/ST/WQ states under bending fatigue and from 0.5% to 3% maximum strain amplitude.

Description of macroscopic failure	CR				CR/573K-0.6ks/WQ CR/573K-7.2ks/WQ				CR/ST/ WQ			
	3%	2%	1%	0.5%	3%	2%	1%	0.5%	3%	2%	1%	0.5%
Not failed				□ (HCF)				O (HCF)				
Partially failed "bended with a visible crack on the tensile face"	□ (LCF)	□ (LCF)	□ (LCF)		Δ (LCF) O (LCF)	Δ (LCF) O (LCF)	Δ (LCF) O (LCF)	Δ (HCF)	◊ (LCF)	◊ (LCF)	◊ (LCF)	◊ (LCF)
Fully failed								Δ (HCF) O (HCF)				

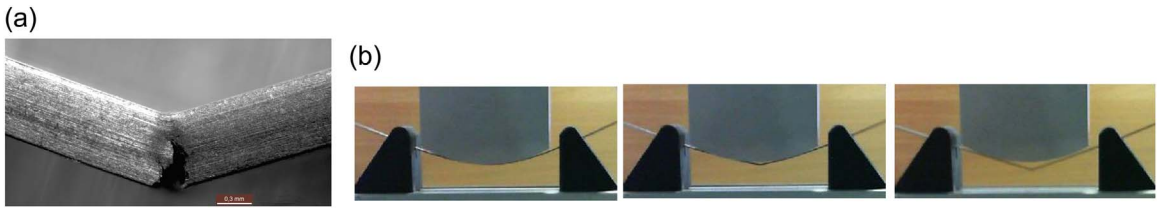

Fig. 5. (a) Macro, example of a specimen after partial fracture - view of the CR/573K-0.6ks/WQ state fatigued at 2% strain amplitude (b) Partial failure bending fatigue, views at 1 min shooting interval (Microsoft HD Camera) - CR/573K-0.6ks/WQ at 0.5% strain.

four CR, CR/573K-0.6ks/WQ, CR/573K-7.2ks/WQ and CR/ST/WQ states under bending fatigue from 0.5% to 3% maximum strain amplitudes. Information as to whether the sample belongs to the LCF or the HCF regime is added.

Most post-mortem samples that are declared failed according to ε/N_f curves show a bended form with a visible crack on their face loaded under tension (Fig. 5a). This is the case in the LCF regime for the four types of microstructure tested. In the HCF regime, the CR/573K-0.6ks/WQ state at 0.5% amplitude strain failed either partially or fully. In the case of the broken piece CR/573K-7.2ks/WQ state at 0.5% amplitude strain, the sample has fully failed.

As illustrated in Fig. 5.b with the sequence of three shots HD camera capturing at 1 min interval, failure occurs quite suddenly.

3.3.3. Fracture surface

SEM observations have been made on 1% fatigue strain postmortem specimens (Fig. 6) for the four states. Damage details are also given on the micrographs.

The bottom and the upper half-thicknesses parts of the micrographs correspond to the parts of sample loaded respectively under tension and compression. According to the bending fatigue mode, the maximum amplitude strain (stress) is on the external faces.

The solution treated specimen (ST) exhibits a damage that seems to propagate in a brittle way (Fig. 6a and Fig. 6a1) on almost the entire surface of the specimen. The austenitic β grains of about 80–100 μm are well observed as well as large parallel lines appearing within these grains (Fig. 6a2). These lines could be interpreted as intragranular twining and/or slip traces. These plastic mechanisms accommodate the deformation once the amount of stress-induced martensite α" appearing during cycling stabilizes. The {332} < 113 > twinning has already been observed for unstable β phase Ti-Nb alloys containing 40 wt% (equivalent to 26 at%) Nb (Hanada et al., 1985). In addition, failure damage is enhanced by the presence of intergranular crack propagation as shown in Fig. 6a3. One can also note the presence of a few fatigue lines (Fig. 6a4) near which equiaxed dimples are observed. All these results are in agreement with the poor fatigue life results (shown on Fig. 4) of the CR/ST/WQ state under bending cycling. The cold-rolled (CR) and cold-rolled aged (CR/573K-0.6ks/WQ, CR/573K-7.2ks/WQ)) specimens exhibit (respectively, Fig. 6b,c and d) more or less wide fast fracture areas of brittle nature above which are observed stable crack propagation zones. Fatigue cracks are always initiated from the tensile surfaces and propagate parabolicaly towards the sample centers and upper sample boards under compression.

For each of these three states (CR, CR/573K-0.6ks/WQ and CR/573K-7.2ks/WQ), the stable crack propagation zone exhibits, perpendicularly to the fast crack propagation direction, equiaxed dimples near fatigue lines (respectively, Fig. 6b2, c3 and d2) which could be responsible for a ductile crack propagation.

While the CR and CR/573K-0.6ks/WQ states have equivalent fatigue performances at 1% strain amplitude (Fig. 4), the cold-rolled short-time-aged state fractography clearly shows additional uniform distributed fatigue striations corresponding to micro secondary cracks (Fig. 6c2). These weakening mechanisms can be analyzed as slip plane decohesions due to the presence of α and isothermal ω intragranular particles acting as an efficient barrier to dislocations movement (Akahori et al., 2005). They could promote fatigue lines as suggested by the comparison of 1% and 3% fatigue strain micrographs realized on CR/573K-0.6ks/WQ (Fig. 6c2, Fig. 6c3 and Fig. 7).

The CR/573K-7.2ks/WQ state exhibits a relatively earlier weakness in the LCF region compared to that of the CR and CR/573K-0.6ks/WQ states (Fig. 4). This can be explained by the presence of additional intergranular craks (Fig. 6d1) and a large proportion of microvoids (Fig. 6d2). The first phenomenon can be related to the decohesion from the β matrix caused by the presence of α particles at β grains boundaries. The second one should probably be explained by the relatively high proportion of (α+ω) particles within the β-grains. This weaknening mechanism can result from a high stress concentration around these numerous nanometric precipitates as from an incoherence with the β-matrix due to a modification of chemical composition in a local way (Hickman, 1969; Lyon, 1981; Hanada et al., 1985; Prima et al., 2000b).

3.3.4. Discussion

As the cold-rolled, cold-rolled-aged and solution treated states exhibit the same relative number of cycles at failure (N_f) in the LCF region (at 1%, 2% and 3% strain), $N_{f\ CR} > N_{f\ CR/573K\text{-}0.6ks/WQ} > N_{f\ CR/573K\text{-}7.2ks/WQ}$ (Fig. 4), the deformation mechanisms that have been proposed for each state at 1% strain can be extended to the other strain amplitudes in this region.

Furthermore, an inversion of the fatigue life performances has been observed in the HCF region (at 0.5%), for the aged states. The CR/573K-7.2ks/WQ state exhibits a higher fatigue performance than that of the CR/573K-0.6ks/WQ state. The relative number of cycles at failure in the HCF region is as follow: $N_{f\ CR} \geq N_{f\ CR/573K\text{-}7.2ks/WQ} > N_{f\ CR/573K\text{-}0.6ks/WQ}$. Under high strain cyclic bending, a relatively high density (α+ω) particles coupled with intergranular 40–60 nm α precipitates have a deleterious effect on the fatigue life while under low strain cyclic bending their influence is less significant.

The fatigue fracture facies of the short time aged (0.6 ks) Ti-26Nb alloy (equivalent in both the LCF and HCF areas) have established that the 10–20 nm ω precipitates do not participate in the embrittlement of the specimen by debonding. The ω particles seem to act as a barrier to dislocation movement.

For the CR/573K-7.2ks/WQ specimen with a high density of both (α+ω) intragranular precipitates and intergranular α phase, two embrittlement mechanisms according to cyclic fatigue area have been proposed.The poor fatigue life of this specimen at high strain amplitudes greater than 1% (LCF) has been related to the interfacial decohesion of the ω precipitates from the matrix and intergranular decohesion due to the α phase. At lower strain amplitude (0.5%), the CR/573K-7.2ks/WQ state can be considered as a severe competitor against the CR state that has not failed and for which the stress-induced-martensite α" (Table 1) is initially present. It has been reported that the longest fatigue life at low strain is obtained for the highly-dislocated and the most strain-hardened states (Sheremetyev et al., 2016). As the ω phase precipitation, which occurs during the aging treatment, anneals further martensitic transformation from β→α" (Ohmori et al., 1998), the good fatigue performances of the CR/573K-7.2ks/WQ state at low strain amplitude can not be explained by

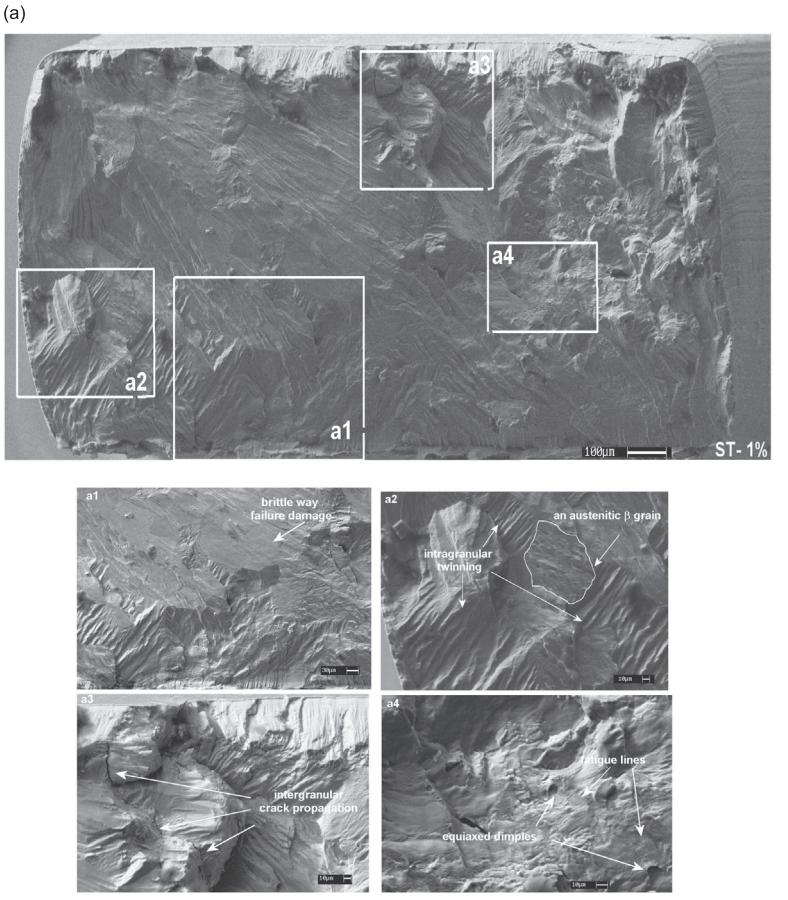

a1 - brittle way failure damage, a2- Intragranular twinning, a3- intergranular crack propagation, a4- Fatigue lines near equiaxed dimples.

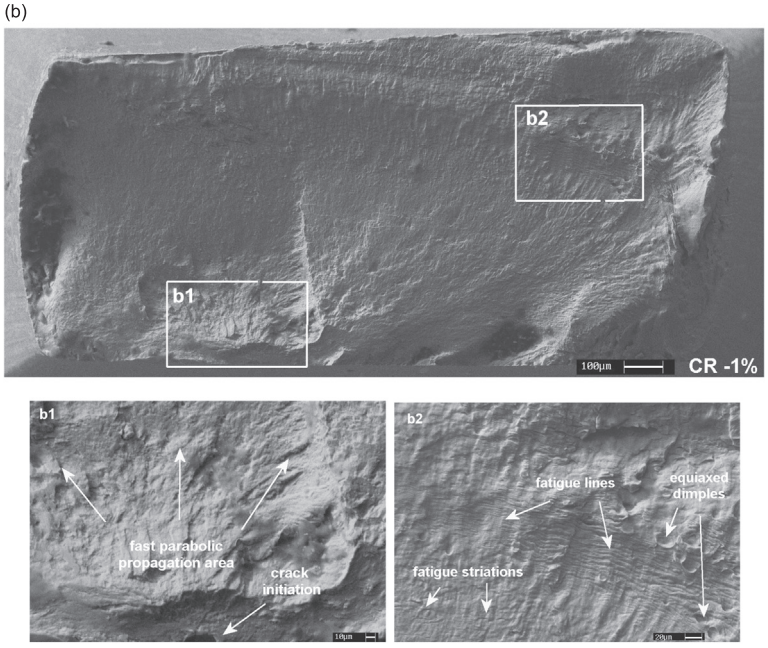

b1-crack initiation and fast parabolic propagation area, b2- stable crack propagation area with fatigue striations and fatigue lines near equiaxed dimples.

Fig. 6. Typical post-mortem SEM micrographs of whole fatigue fracture surface at 1% strain amplitude (LCF life region) for the (a) CR/ST/WQ, (b) CR, (c) CR/573K-0.6ks/WQ and (d) CR/573K-7.2ks/WQ states with focus on some damage details for each state.

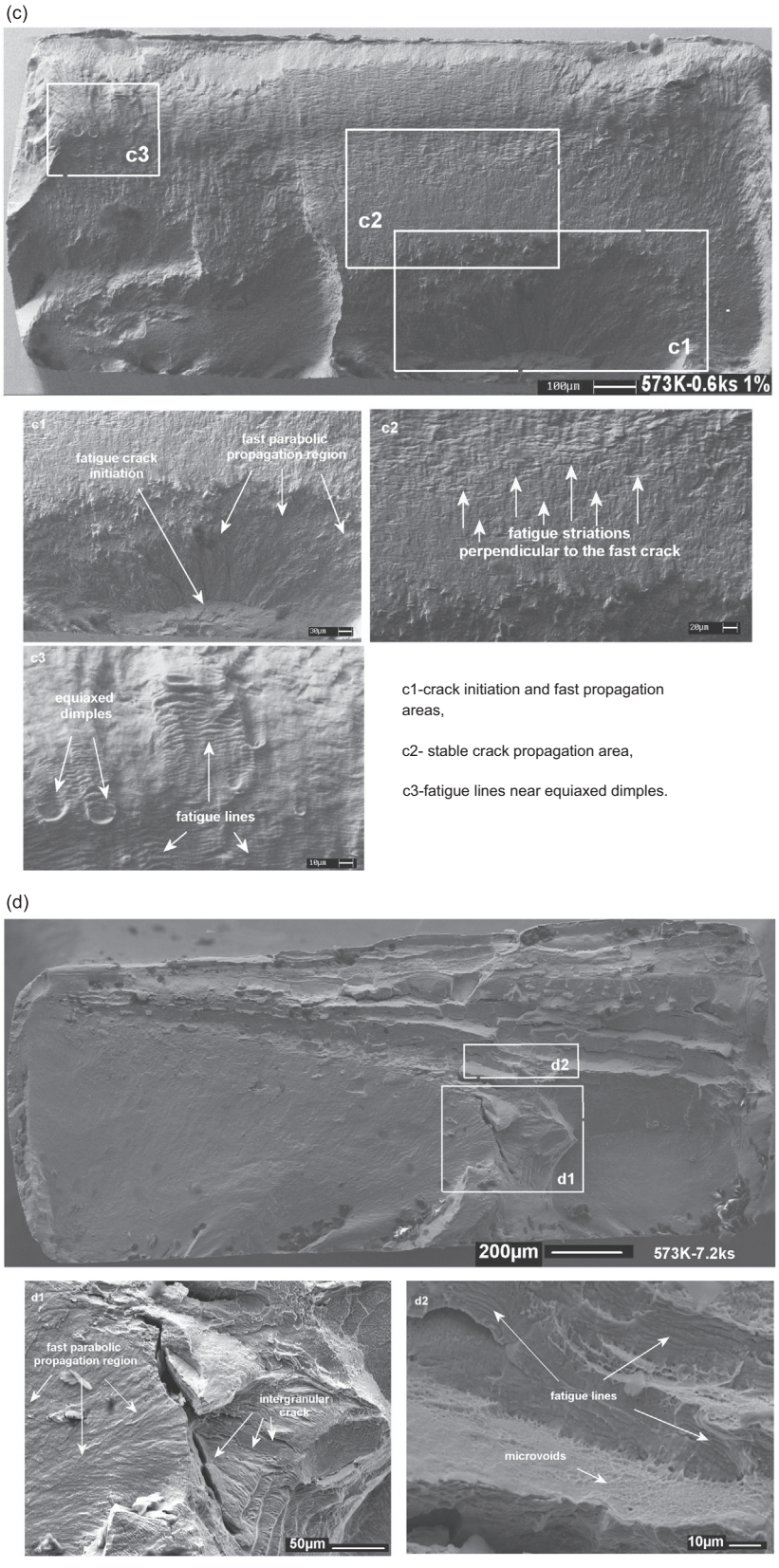

Fig. 6. (*continued*)

the reversible β↔α" stress-induced phase transformation, corresponding to a pseudoelasticity behavior in the loading-unloading process of the fatigue tests, as it could be suggested for the CR state. Indeed, this explanation can be supported by the results of tensile cycling tests conducted on a high cold rolled metastable β TiNbSn alloy showing a (β+α") structure in the elastic part of its stress-strain curve (low strain). These results exhibit a pseudoelastic behavior that has been related to the rearrangement of martensite variants formed by cold rolling and/or

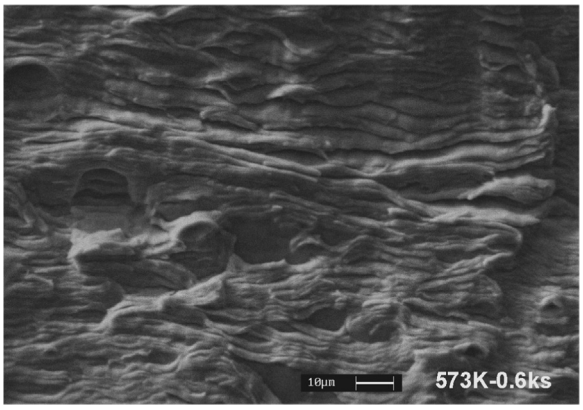

Fig. 7. Fatigue lines near equiaxed dimples for CR/573K-0.6ks/WQ state at 3% strain amplitude.

stress-induced martensitic transformation in the retained β phase (Matsumoto et al., 2007). Considering that the CR/573K-7.2ks/WQ state exhibits the highest Young's modulus and the highest critical stress for slip, it is suggested that the local micro-stresses around the α and ω precipitates at low straining amplitude could remain below these threshold constraints, involving elastic deformation (Sheremetyev et al., 2016).

4. Conclusion

The biocompatible metastable β-titanium Ti-26Nb alloy was the subject of the present study. In order to use it for medical applications as prosthesis and implants, it has to present a high resistance associated with an elastic modulus close to that of the cortical bone, as well as good fatigue performances. The principal aim of this work was to comparatively examine the influence of the microstructure on the performances under fatigue and under static tensile. For medical applications type hip-joint, it is reported that fatigue loadings at low strain amplitude (< 1%) are representative. The main findings are as follows:

1) Cold rolling process produces β+α" phase microstructure to which is associated a low Young's modulus of 54 GPa and a critical stress for slip of 900 MPa. At low straining amplitude, this state does not fail, which is explained by successive loading unloading in the domain of the β↔α" transformation,
2) The ST alloy with a single β phase has a low Young's modulus of 48 GPa and a recoverable tensile strain of 2%, and its superelasticity is largely due to the reversible phase. Its fatigue life does not exceed one hundred thousand cycles, limiting it for medical applications,
3) The cold rolled alloy aged at low temperature exhibits an intragranular (ω+α) phases whose volume fraction increases with the holding time. An additional precipitation of intergranular α phase at the β grains boundaries was observed for the longest isothermal holding time. For quasi-static tensile tests, the microstructure associated to the longer time aging induces an increase of the Young's modulus and the critical stress, and makes the material brittle after 2.6% strain amplitude. The low straining tends to minimize the two proposed embritlement mechanisms related to the interfacial decohesion of the ω precipitates from the matrix and to the intergranular decohesion due to the α phase observed at the β grains boundaries.

In conclusion, the best fatigue life performances of the Ti-26Nb alloy at low strain amplitude are obtained through either a severe cold deformation or a long-time aged material at low temperature inducing respectively stress-induced martensite α" and high density of intragranular nanometric precipitates associated to intergranular α precipitates.

For biomedical applications the cold-hyperdeformed state will be favoured as compared to the solution-treated and aged states according to its Young's modulus, which is much closer to that of the bone.

References

Akahori, T., Niinomi, N., Fukui, H., Ogawa, M., Toda, H., 2005. Improvement in fatigue characteristics of newly developed beta type titanium alloy for biomedical applications by thermo-mechanical treatments. Mater. Sci. Eng. C 25, 248–254.
Azimzadeh, S., Rack, H.J., 1998. Phase transformations in Ti-6.8Mo-4.5Fe-1.5Al. Metall. Mater. Trans. A 29A, 2455–2467.
Bahia, M.G.A., Dias, R.F., Buono, V.T.L., 2006. The influence of high amplitude cycling straining on the behaviour of superelastic NiTi. Int. J. Fat. 28, 1087–1091.
Boehlert, C.J., Cowen, C.J., Jaeger, C.R., Niinomi, M., Akahori, T., 2005. Tensile and fatigue evaluation of Ti-15Al-33Nb (at.%) and Ti-21Al-29Nb (at.%) alloys for biomedical applications. Mater. Sci. Eng. C 25, 263–275.
Boehlert, C.J., Cowen, C.J., Quas, t J.P., Akahori, T., Niinomi, M., 2008. Fatigue and wear evaluation of Ti-Al-Nb alloys for biomedical applications. Mater. Sci. Eng. C 28, 323–330.
Bourauel, C., Scharold, W., Jäger, A., Eliades, T., 2008. Fatigue failure of as-received and retrieved NiTi orthodontic archwires. Dent. Mater. 24, 1095–1101.
Bowen, A.W., 1971. Omega phase embrittlement in aged Ti-15%Mo. Scr. Mater. 5, 709–716.
Duerig, Terlinde, Williams, D.F., 1980. The ω-phase reaction in titanium alloy. In: Proceedings of the 4th International conference on titanium 2, 1299–1308.
Eggeler, G., Hornbogen, E., Yawny, A., Heckmann, A., Wagner, M., 2004. Structural and functional fatigue of NiTi shape memory alloys. Mater. Sci. Eng. A 378, 24–33.
Elmay, W., Prima, F., Gloriant, T., Bolle, B., Zhong, Y., Patoor, E., Laheurte, P., 2013. Effects of thermomechanical process on the microstructure and mechanical properties of a fully martensitic titanium-based biomedical alloy. J. Mech. Behav. Biomed. Mater. 18, 47–56.
Elmay, W., Patoor, E., Gloriant, T., Prima, F., Laheurte, P., 2014. Improvement of superelastic performance of Ti-Nb binary alloys for biomedical applications. J. Mater. Eng. Perform. 23, 2471–2476.
Figueiredo, A.M., Modenesi, P., Buono, V., 2009. Low-cycle fatigue life of superelastic NiTi wires. Int. J. Fat. 31, 751–758.
Froes, F.H., Yolton, C.F., Capenos, J.M., Wells, M.G.H., Williams, J.C., 1980. The relationship between microstructure and age hardening response in the metastable beta titanium alloy Ti-11.5Mo-6Zr-4.5Sn (beta III). Metall. Trans. A 11A, 21–31.
Frotscher, M., Nörtershäuser, P., Somsen, Ch, Neuking, K., Böckmann, R., Eggeler, G., 2009. Microstructure and structural fatigue of ultra-fine grained NiTi-stents. Mater. Sci. Eng. A 503, 96–98.
Furuhara, T., Maki, T., Makino, T., 2001. Microstructure control by thermomechanical processing in β-Ti-15-3 alloy. J. Mater. Tech. 117, 318–323.
Geetha, M., Singh, A.K., Asokamani, R., Gogia, A.K., 2009. Ti based biomaterials, the ultimate choice for orthopaedic implants - a review. Prog. Mater. Sci. 54, 397–425.
Guo, Q., Zhan, Y., Mo, H., Zhang, G., 2010. Aging response of the Ti–Nb system biomaterials with β-stabilizing elements. Mater. Des. 31, 4842–4846.
Hao, Y.L., Li, S.J., Sun, S.Y., Zheng, C.Y., Yang, R., 2007. Elastic deformation behaviour of Ti-24Nb-4Zr-7.9Sn for biomedical applications. Acta Biomater. 3, 277–286.
Hanada, S., Ozeki, M., Izumi, O., 1985. Deformation characteristics in β phase Ti-Nb alloys. Metall. Trans. A 16A, 789–795.
Hanada, S., Matsumoto, H., Watanabe, S., 2005. Mechanical compatibility of titanium implants in hard tissues. Int. Congr. Ser. 1284, 239–247.
Hickman, B.S., 1969. The formation of omega phase in titanium and zirconium alloys: a review. J. Mater. Sci. 4, 554–563.
Kent, D., Wang, G., Yu, Z., Dargusch, M.S., 2010. Pseudoelastic behaviour of a β Ti-25Nb-3Zr-3Mo-2Sn alloy. Mater. Sci. Eng. A 527, 2246–2252.
Kim, H.Y., Kim, J.I., Inamura, T., Hosoda, H., Miyazaki, S., 2006. Effect of thermomechanical treatment on mechanical properties and shape memory behavior of Ti-(26-28) at.% Nb alloys. Mater. Sci. Eng. A 438-440, 839–843.
Kim, H.S., Lim, S.H., Yeo, I.D., Kim, W.Y., 2007. Stress-induced martensitic transformation of metastable β-titanium alloy. Mater. Sc. Eng. A 449-451, 322–325.
Larson, F.R., Zarkades, A., 1974. MCIC Report, 74-20.
Li, S.J., Jia, M.T., Prima, F., Hao, Y.L., Yang, R., 2011. Improvements in nonlinear elasticity and strength by grain refinement in a titanium alloy with high oxygen content. Scr. Mater. 64, 1015–1018.
Liu, Y., Xiang, H., 1998. Apparent modulus of elasticity of near-equiatomic NiTi. J. Alloy. Compd. 270, 154–159.
Lyon, O., 1981. La formation de phase ω isothermal dans l'alliage Ti-35wt.%Nb étudiée par microscopie électronique et par diffusion de rayons X aux petits angles. J. Less-Common Met. 81, 103–113.
Matsumoto, H., Watanabe, S., Hanada, S., 2007. Microstructures and mechanical properties of metastable β TiNbSn alloys cold rolled and heat treated. J. Alloy. Compd. 439, 146–155.
Miyazaki, S., Mizukoshi, K., Ueki, T., Sakuma, T., Liu, Y., 1999. Fatigue life of Ti-50 at.% Ni and Ti-40Ni-10Cu (at.%) shape memory alloy wires. Mater. Sci. Eng. A 273-275, 658–663.
Miyazaki, S., Kim, H.Y., Hosoda, H., 2006. Development and characterization of Ni-free Ti-base shape memory and superelastic alloys. Mater. Sci. Eng. A 438-440, 18–24.
Moffat, D.L., Larbalestier, D.C., 1988. The competition between the alpha and omega phases in aged Ti-Nb alloys. Metall. Trans. A 19A, 1687–1694.
Morita, A., Fukui, H., Tanado, H., Hayashi, S., Hasegawa, J., Niinomi, M., 2000. Alloying titanium and tantalum by cold crucible levitation melting (CCLM) furnace. Mater.

Sci. Eng. A 280, 208–213.
Niinomi, M., 2003. Fatigue performance and cyto-toxicity of low rigidity titanium alloy, Ti-29Nb-13Ta-4.6Zr. Biomaterials 24, 2673–2683.
Niinomi, M., 2007. Fatigue characteristics of metallic biomaterials. Int. J. Fat. 29, 992–1000.
Niinomi, M., Akahori, T., Katsura, S., Yamauchi, K., Ogawa, M., 2007. Mechanical characteristics and microstucture of drawn wire of Ti-29Nb-13Ta-4.6Zr for biomedical application. Mater. Sci. Eng. C 27, 154–161.
Niinomi, M., Nakai, M., 2011. Titanium-Based biomaterials for preventing stress shielding between implant devices and bone. Int. J. Biomater.. http://dx.doi.org/10.1155/2011/836587.
Niinomi, M., Nakai, M., Hieda, J., 2012. Development of new metallic alloys for biomedical applications. Acta Biomater. 8, 3888–3903.
Ohmori, Y., Natsui, H., Nakai, K., Ohtsubo, H., 1998. Effects of ω phase formation on decomposition of α"/β duplex phase structure in a metastable β Ti Alloy. Mater. Trans. JIM 39, 40–48.
Ohmori, Y., Ogo, T., Nakai, K., Kobayashi, S., 2001. Effects of ω-phase precipitation on β→α, α" transformations in a metastable β titanium alloy. Mater. Sci. Eng. A 312, 182–188.
Pelton, A.R., Fino-Decker, J., Vien, L., Bonsignore, C., Saffari, P., Launey, M., Mitchell, M.R., 2013. Rotary-bending fatigue characteristics of medical-grade Nitinol wire. J. Mech. Behav. Biomed. Mater. 27, 19–32.
Prima, F., Debuigne, J., Boliveau, M., Ansel, D., 2000a. Control of omega phase volume fraction precipitated in a beta titanium alloy: development of an experimental method. J. Mater. Sci. Lett. 19, 2219–2221.
Prima, F., Vermaut, P., Ansel, D., Debuigne, J., 2000b. ω precipitation in a beta metastable titanium alloy, resistometric study. Mater. Trans. JIM 41, 1092–1097.
Prima, F., Vermaut, P., Texier, G., Ansel, D., Gloriant, T., 2006. Evidence of a-nanophase heterogeneous nucleation from x particles in a b-metastable Ti-based alloy by high-resolution electron microscopy. Scr. Mater. 54, 645–648.
Sauer, C., Luetjering, G., 2001. Thermo-mechanical processing of high strength β-titanium alloys and effects on microstructure and properties. J. Mater. Proc. Tech. 117, 311–317.
Sheremetyev, V., Brailovski, V., Prokoshkin, S., Inaekyan, K., Dubinskiy, S., 2016. Functional fatigue behavior of superelastic beta Ti-22Nb-6Zr(at%) alloy for load-bearing biomedical applications. Mater. Sci. Eng. C 58, 935–944.
Silcock, J.M., 1958. An X-Ray examination of the ω phase in TiV, TiMo and TiCr alloys. Acta Metall. 6, 481–493.
Song, X., Wang, L., Niinomi, M., Nakai, M., liu, Y., 2015. Fatigue characteristics of a biomedical β-type titanium alloy with titanium boride. Mater. Sci. Eng. A 640, 154–164.
Sun, F., Hao, Y.L., Nowak, S., Gloriant, T., Laheurte, P., Prima, F., 2011. A thermo-mechanical treatment to improve the superelastic performances of biomedical Ti-26Nb and Ti-20Nb-6Zr (at.%) alloys. J. Mech. Behav. Biomed. Mater. 4 (1), 1864–1872.
Tahara, M., Kim, H.Y., Hosoda, H., Miyazaki, S., 2009. Cyclic deformation behavior of a Ti-26 at.% Nb alloy. Acta Mater. 57, 2461–2469.
Wagner, M., Sawaguchi, T., Krausträter, G., Höffken, D., Eggeler, G., 2004. Structural fatigue of pseudoelastic NiTi shape memory wires. Mater. Sci. Eng. A 378, 105–109.
Williams, D.F., 2008. On the mechanisms of biocompatibility. Biomaterials 29, 2941–2953.
Williams, J.C., Hickman, B.S., Marcus, H.L., 1971. The effect of omega phase on the mechanical properties of titanium alloys. Metall. Trans. 2, 1913–1919.
Windler, M., Klabunde, R., 2001. Titanium for hip and knee prostheses. In: Brunette, D.M., Tengvall, P., Textor, P., Thomson, P. (Eds.), Titanium in Medicine. Springer, 710.
Xu, T.W., Zhang, S.S., Zhang, F.S., Kou, H.C., Li, J.S., 2016a. Effect of ω-assisted precipitation on β→α transformation and tensile properties of Ti–15Mo–2.7Nb–3Al–0.2Si alloy. Mater. Sci. Eng. A 654, 249–255.
Xue, H.Q., Tao, H., Montembault, F., Wang, Q.Y., Bathias, C., 2007. Development of a three-point bending fatigue testing methodology at 20 kHz frequency. Inter. J. Fat. 29, 2085–2093.
Young, J.M., Van Vliet, K., 2005. Predicting In Vivo failure of pseudoelastic NiTi devices under low cycle, high amplitude fatigue. J. Biomed. Mater. Res. B Appl. Biomater., 17–26.
Zhang, S.Q., Li, S.J., Jia, M.T., Hao, Y.L., Yang, R., 2009. Fatigue properties of a multifunctional titanium alloy exhibiting nonlinear elastic deformation behavior. Scr. Mater. 60, 733–736.